Microstructures and Properties of Carburized Steels

George Krauss
Advanced Steel Processing and Products Research Center
Colorado School of Mines

Reprinted from
METALS HANDBOOK®
Volume 4: Heat Treating

REPRINT

ASM INTERNATIONAL®
The Materials Information Society

ASM International® is a Society whose mission is to gather, process and disseminate technical information. ASM fosters the understanding and application of engineered materials and their research, design, reliable manufacture, use and economic and social benefits. This is accomplished via a unique global information-sharing network of interaction among members in forums and meetings, education programs, and through publications and electronic media.

SAN:204-7586

ASM International®
Materials Park, Ohio 44073

Printed in the United States of America

Microstructures and Properties of Carburized Steels

George Krauss, Advanced Steel Processing and Products Research Center, Colorado School of Mines

CARBURIZING is a remarkable method of enhancing the surface properties of shafts, gears, bearings, and other highly stressed machine parts. Low-carbon steel bars are fabricated, by forging and machining, into finished shapes and then are converted by carburizing into a composite material consisting of a high-carbon steel case and low-carbon steel core. When this steel composite is quenched to martensite and tempered, the high hardness and strength of the case microstructure, combined with the favorable case compressive residual stress developed by interactions between the case and core during quenching, produce very high resistance to wear, bending fatigue, and rolling-contact fatigue.

The furnaces, atmospheres, control, and kinetics of carburizing are described in other articles in this Volume. The purpose of this article is to describe the microstructure, properties, and performance of carburized steels. At first glance, the microstructures of carburized steels appear to be quite straightforward: high-carbon martensite gradually replaced by martensite of lower carbon content with increasing distance from the carburized surface. This view of the microstructures of carburized steel is essentially correct. Lightly tempered martensite is the dominant microstructural constituent of properly carburized steel. However the martensite changes in morphology, amount, and properties as a function of distance from the surface. Other microstructural constituents may also be present and may significantly affect the performance of carburized parts. These other microstructural components include retained austenite; carbides of various origins, sizes, and morphologies; inclusions; processing-induced surface oxides; prior austenite grain boundaries embrittled by phosphorus segregation; and nonmartensitic transformation products of austenite, such as bainite and pearlite.

Because most carburized parts are subjected to cyclic loading, by far the most important property or measure of their performance is fatigue resistance. Hardness is another property commonly measured in carburized steels and is used as a quality control parameter to document carburizing success and to establish case depths. However, although many carburized steels have the same hardness profiles, they may have different microstructures and perform quite differently. Mechanical properties as measured by tensile testing are of little value because of the gradients in microstructures and properties between the surface and center of carburized steels. Thus strength and fracture toughness, which are useful in estimating critical flaw or crack sizes, are largely inferred from measurements on through-hardened steels of medium and high carbon content, although some measurements of fracture toughness have been made on carburized specimens (Ref 1, 2).

Throughout this article, the various microstructural components are described. Where possible, the effect of microstructure on properties, primarily hardness and fatigue resistance, are incorporated into the discussion of a particular microstructural feature.

Much of the published work on carburizing is devoted to processing (Ref 3, 4), aided by computer modelling and control technology (Ref 5, 6). Nevertheless, the understanding of the role microstructure plays in optimizing the performance of carburized steels continues to grow. Parrish thoroughly reviewed microstructures and properties of carburized steels up to 1977 (Ref 7) and, with Harper, authored a comprehensive treatment of all aspects of gas carburizing (Ref 8). An atlas of the microstructures of carburized steels has also been published (Ref 4). Proceedings of recent conferences on carburizing include articles on structure-property correlations as well as processing advances (Ref 1, 5, 6). The above list of major references is far from exhaustive, especially in view of the many articles published in journals, but it provides a good starting point for readers interested in more information regarding the processing, selection, and performance of carburized steels.

Carbon and Hardness Profiles

The object of carburizing is to produce a high-hardness, high-carbon case on a low-carbon steel core with low-to-medium hardness. This objective is accomplished by the introduction of carbon into austenite by various gas-metal surface reactions (Ref 9, 10) and the diffusion of carbon through the austenite from the surface into the core (Ref 9, 11). The austenite is then quenched and is converted to microstructural gradients by solid-state phase transformations during cooling. The microstructural gradients in turn produce hardness gradients. Figures 1 and 2 show, respectively, typical carbon and hardness gradients from test bars of gas-carburized SAE 8620 steel. The microstructural gradients associated with such carbon and hardness gradients are described in the section below. Residual-stress gradients, which develop because of transformation and temperature gradients during quenching, are described in the section "Residual Stresses" in this article.

Case Depth Measurement. There are several ways to measure the depth of the case produced by a given carburizing schedule (Ref 4). Total case depths can be estimated from etching differences between the case and core. One of the most commonly accepted techniques is to section a part or test bar and measure the hardness profile. The perpendicular distance from the surface to the point where the hardness drops to a given hardness, often specified as 50 HRC (510 HV), is defined as the case depth (see the article "Methods of Measuring Case Depth" in this Volume for further information).

Factors Affecting Case Depth. Many factors, especially those that control surface carbon concentration, such as time and temperature during the various stages of a carburizing process, affect case depth. Frequently the first stage of carburizing intro-

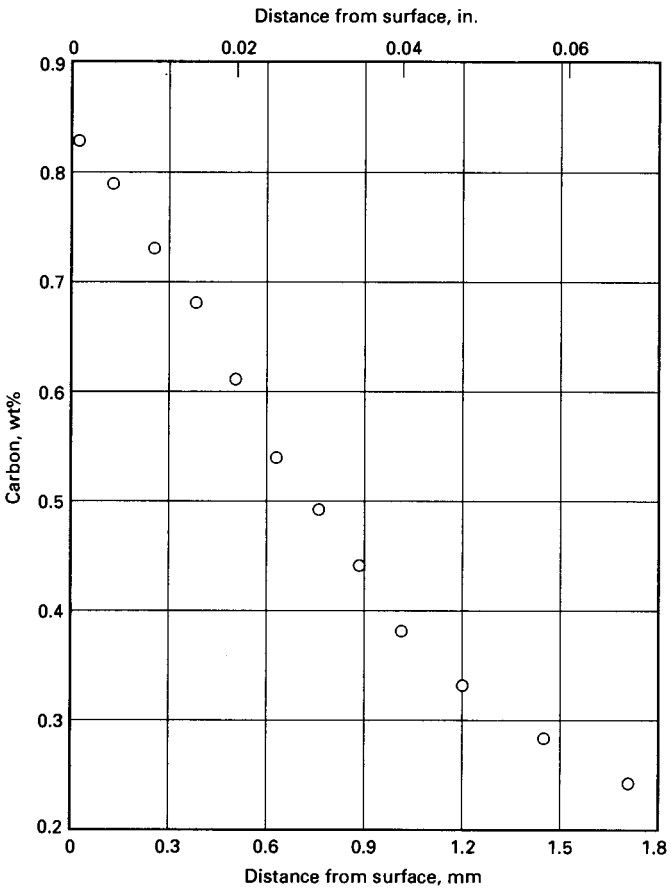

Fig 1 Carbon gradient in a 25 mm (1 in.) diam test bar of 8620 steel after gas carburization at 925 °C (1700 °F). Source: Ref 12

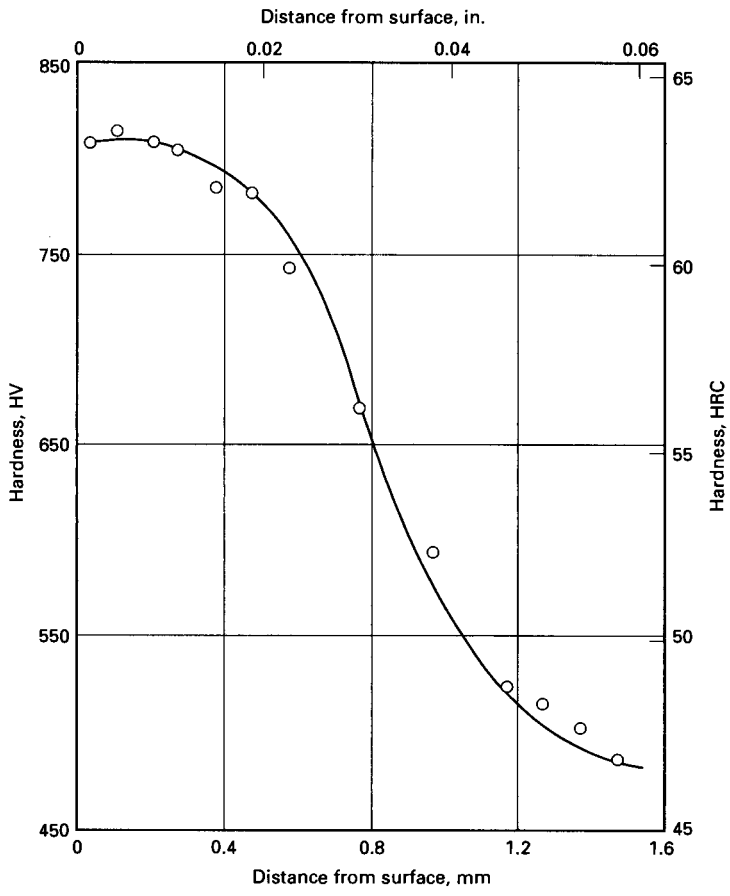

Fig 2 Microhardness profile of 16 mm (0.63 in.) test bar of 8620 steel after gas carburization at 925 °C (1700 °F). Source: Ref 12

duces a high surface carbon content, on the order of 1.1 to 1.2 wt%, depending on the maximum solubility of carbon in austenite at the temperature of that stage. Such carbon contents would produce undesirable quenched microstructures. Therefore to produce optimum surface carbon concentrations of 0.8 to 0.9%, the second stage of carburizing is performed with lower carburizing atmosphere carbon potentials. Carbon already introduced in the first stage then adjusts to the lower surface potential and also diffuses deeper into the core. This two-stage approach is commonly referred to as the boost-diffuse method of carburizing.

Hardenability, as measured by the hardness method, also affects case depths. Generally, it is assumed that austenite of a given carbon concentration transforms to martensite of a given hardness. However, in carburizing steels with low hardenability or in massive carburized parts, which cool slowly, the austenite may transform to bainitic or pearlitic microstructures of lower hardness than martensite. Therefore, identical carbon gradients may produce quite different hardness gradients, depending on hardenability considerations.

Part shape or geometry also affects case depth. Access of the carburizing atmosphere or the quench severity may be affected by complex part shapes. For example the case depths of carburized gear teeth vary between the pitch line and root areas. Figure 3 shows recommended locations for hardness traverses and core hardness measurements for gear teeth, and Fig 4 shows differences in pitch line and root traverses for a carburized 8620H gear. The effective case depth is less at the root than at the pitch line.

Martensite and Austenite

Figure 5 shows the typical martensite-austenite microstructure formed close to the surface of carburized steels quenched directly after carburizing. The high-carbon martensite (dark) is formed by a diffusionless, shear transformation of the austenite and has a morphology characterized by nonparallel plate-shaped crystals (Ref 15, 16). The martensite plates have $\{225\}_A$ and $\{259\}_A$ habit planes with many equivalent variants and therefore assume the many orientations shown in the micrograph. The sizes of the martensite plates are determined by the austenite grain size and the continuous formation of additional plates with decreasing temperature. The first plates form at the martensite start (M_s) temperature and span the austenite grains; the longest dimension of these plates is therefore equivalent to the austenitic grain size. With decreasing temperature, more martensite plates form between large plates, and they become finer as the austenite is increasingly partitioned by more transformation. According to this sequence of martensite formation, the finer the austenite grain size, the finer is the array of martensite plates.

The white areas of Fig 5 are regions of austenite that have not transformed. This austenite is referred to as retained austenite and is present because of the high stability of high-carbon austenite. Increasing carbon content significantly lowers M_s temperatures and depresses the entire temperature range for martensitic transformation to below room temperature. Consequently there are always significant amounts of retained austenite in the cases of carburized steels quenched to room temperature. Retained austenite plays a significant role in the fatigue of carburized steels, as discussed below, and amounts on the order of 30 to 35% are common in the near-surface cases of specimens quenched directly after carburizing.

Carburized parts may be cooled to room temperature after carburizing and reheated for hardening (Ref 17). Such reheating treat-

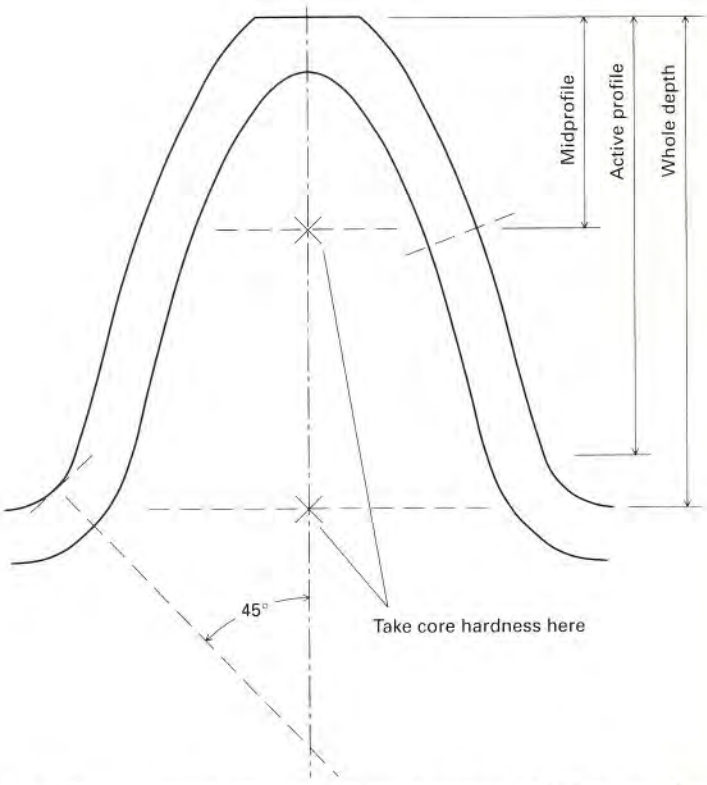

Fig 3 Recommended locations for hardness traverses (dashed lines normal to tooth surface at midprofile, the pitch line, and root radius) and core hardness measurements of a gear tooth. Source: Ref 13

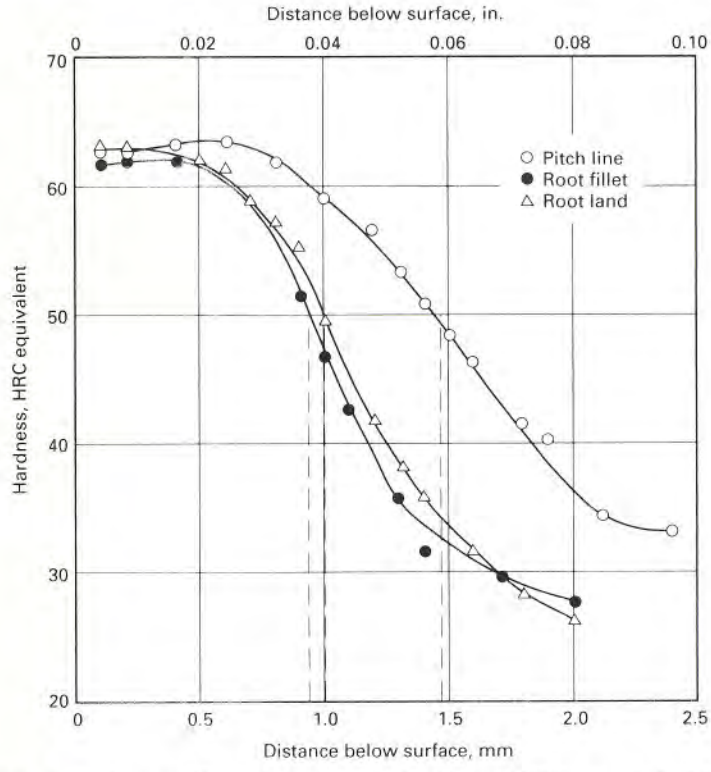

Fig 4 Hardness profiles and effective case depths at 50 HRC for root and pitch line locations of a carburized and hardened 8620H steel gear. Source: Ref 4

ments invariably refine austenitic grain size. If reheating is performed above A_{cm}, that is, the temperature that defines the boundary between the austenite and austenite-cementite phase fields in steels, the structure is completely converted to austenite. Grain size is kept fine by setting austenitizing temperatures just above A_{cm}.

Reheating carburized steels below A_{cm} causes spheroidized carbides to be retained in the case austenite. As a result, the carbon content of the austenite is reduced, M_s is increased, and the quenched microstructure has less retained austenite. Also the carbide particles inhibit grain growth and maintain very fine austenitic grain sizes. Figure 6 shows a martensite-carbide microstructure formed by reheating and quenching a carburized 8620 steel. The small, white, spherical particles are carbides retained during austenitizing and quenching. The matrix structure etches dark and consists of martensite and retained austenite too fine for resolution in the light microscope.

The hardness and strength of martensite increase with increasing carbon content (Ref 16). Therefore the highest hardness of a hardened carburized steel is at or close to the surface. Hardness may peak at a distance from the surface if large amounts of retained austenite, which is much softer than martensite, offset the high hardness of martensite immediately adjacent to the surface where the carbon content, and therefore the retained-austenite content, are at their highest levels. With increasing distance from the carburized surface, the carbon concentration of the martensite decreases, and hardness drops (Fig 2 and 4). Retained austenite also decreases with increasing distance from the surface; as the carbon concentration of the austenite decreases (Fig 1), the M_s temperature increases and more martensite forms on cooling to room temperature. Figure 7 shows retained austenite gradients in direct-quenched and reheated carburized 8620 steel specimens. The dramatic reduction of retained austenite content as a result of reheating below A_{cm} (double reheat) is apparent.

The core microstructures of carburized steels are determined by the low carbon content and base hardenability of the carburizing steel. If the steel has low hardenability, the low-carbon core may transform to ferrite and small amounts of pearlite, depending on quench rate. If the steel has high hardenability, the core may transform to martensite. For most highly stressed applications, a martensitic core is desired. Low-carbon martensite has higher strength and fracture resistance or toughness than do ferrite-pearlite microstructures. This increased strength is necessary to prevent

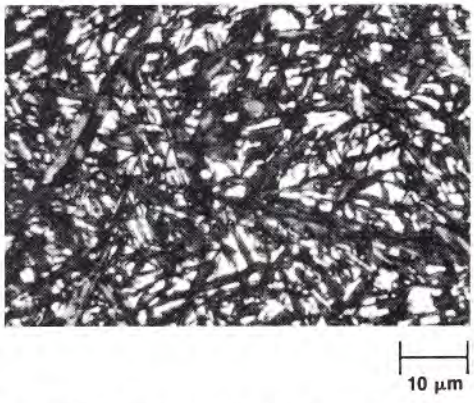

Fig 5 Plate martensite-austenite microstructure in case of carburized and direct-quenched SAE 4121 (formerly EX24 steel) (0.89Mn-0.55Cr-0.24Mo). Light micrograph. Source: Ref 14

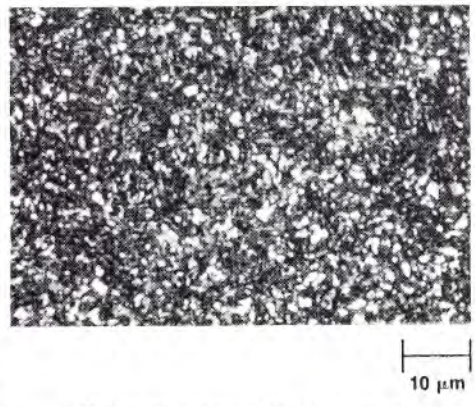

Fig 6 Martensite-dispersed carbide microstructure in case of reheated and quenched carburized 8620 steel. The carbides are the circular, white features dispersed in the dark, martensitic matrix. Light micrograph. Source: Ref 14

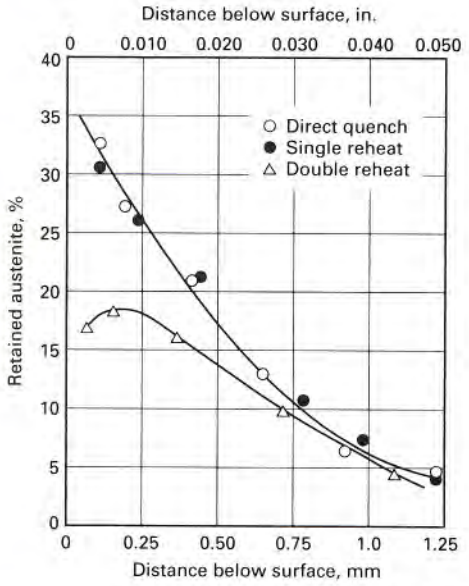

Fig 7 Retained austenite, measured by x-ray diffraction, as a function of distance from the surface of an 8620 steel carburized at 925 °C (1700 °F). The single and double reheats were accomplished by heating to 845 and 790 °C (1550 and 1450 °F), respectively. Source: Ref 18

subsurface crack initiation, sometimes referred to as case crushing (Ref 8, 13, 19). This mode of fracture occurs at case-core interfaces when heavy contact loads create stresses that exceed the strength of the microstructure at some distance below the surface. Subsurface crack initiation is prevented by producing deeper cases by carburizing for longer times, by using alloy steels with higher base hardenability that transform completely to martensite in the core as well as the case, or by increasing core carbon content. Thus strength is raised above applied stresses at critical subsurface locations.

Figure 8 shows the martensitic core microstructure of a carburized steel containing 1.06% Mn, 0.52% Cr, 0.50% Ni, and 0.17% Mo. The low-carbon martensite is referred to as lath martensite, and the morphology consists of fine laths arranged parallel to one another in regions termed packets (Ref 15, 16). The packets are visible in the light microscope, but most of the laths or individual crystals of martensite are too fine to be resolved by light microscopy.

As-quenched carburized steels are generally tempered between 150 and 200 °C (300 and 400 °F). This final heat treatment step increases toughness slightly and relieves some residual stresses, but case hardness and compressive residual stresses are largely preserved. These changes in properties are accomplished by very fine scale changes of the microstructure. The major change consists of the precipitation of a transition carbide from the martensite supersaturated with carbon by quenching (Ref 16). This carbide, termed eta (η)-carbide, has been

Fig 8 Lath martensite microstructure in core of gas-carburized type 8719 steel containing 1.06% Mn, 0.52% Cr, 0.50% Ni, and 0.17% Mo. Light micrograph. Source: Ref 20

shown to have an orthorhombic crystal structure and to precipitate in rows of very fine particles, about 2 nm in size, within the martensite plates. These microstructural changes are much too fine to be resolved in the light microscope, but are reflected by an increased tendency of the martensite plates to appear black after etching. Retained austenite is not transformed by tempering at temperatures of 200 °C (400 °F) or lower. Therefore, the typical polished and etched case structure of a carburized steel consists of dark-etching martensite in a matrix of retained austenite, as shown in Fig 5.

Figure 9 shows impact and fracture toughness measured for hardened 52100 steel as a function of tempering temperature. The microstructures consisted of retained carbides in a matrix of tempered martensite, typical of that formed in bearing steels or in the surface of carburized steel reheated below the A_{cm} (Fig 6). The toughness of the 52100 steel was low, even after tempering at 200 °C (400 °F). Other studies show that plane-strain fracture toughness (K_{Ic}) for high-carbon martensite-austenite microstructures tempered between 150 and 200 °C (300 and 400 °F), equivalent to the near-surface case microstructures of carburized steels, ranges between 15 and 25 MPa$\sqrt{m}$ (14 and 23 ksi$\sqrt{in.}$) (Ref 22).

Alloying Effects

The primary concern in alloy development and the selection of carburizing steels is hardenability. In carburizing steels, a given composition must provide adequate hardenability over a range of carbon contents because hardenability is important for both the case region and the core (see the article "Introduction to Surface Hardening of Steels" in this Volume). The objective is to produce a high-carbon martensitic case (for wear and fatigue resistance) and a low-carbon martensitic core to provide sufficient strength to resist case-core failures as described previously.

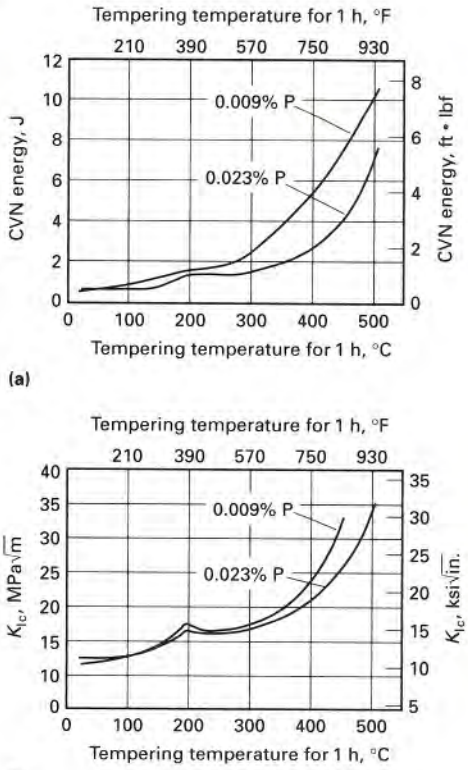

Fig 9 Toughness of 52100 steel (oil quenched from 850 °C, or 1560 °F) with microstructures of dispersed spherical carbides in tempered martensite similar to microstructures formed in the case of carburized steels reheated below A_{cm}. (a) Charpy V-notch impact energy. (b) Plane-strain fracture toughness (K_{Ic}). Source: Ref 21

The goal of hardenability is the formation of hard martensite in preference to microstructures of lower hardness (Ref 16, 23, 24). The controlling factors may be metallurgical, such as the effects of substitutional alloying elements that retard solid-state, diffusion-controlled transformation of austenite to bainite, pearlite, or ferrite; or they may be technological, such as the selection of quenchants, or compensating for slow cooling rates in heavy sections, which provide time for diffusion-controlled transformation at the expense of martensitic transformation. The alloying elements traditionally used for improving hardenability in carburized steels are manganese, chromium, molybdenum, and nickel. Combinations of moderate amounts of several elements have been found to be more effective than large amounts of a single element. Boron is most effective in improving the hardenability of low-carbon steels but loses its effectiveness as carbon content increases. Therefore, it is not expected to improve case hardenability. However, a German carburizing steel, 20MnCr5B, uses boron to remove nitrogen from solution and thereby improve toughness (Ref 25).

Most carburizing steels are deoxidized with aluminum for grain size control. Alu-

minum combines with nitrogen to form aluminum nitride particles, which limit austenite grain growth during carburizing (Ref 16). Fine grain size reduces hardenability, and Cook has shown that the case hardenability of plain carbon steels is reduced because of the grain-refining effect of aluminum additions (Ref 26). This effect of aluminum on hardenability is not noted in alloy carburizing steels.

Alloy Effects on Hardenability. Hardenability is important for both the case and core regions of carburized steels, and a given steel must have adequate hardenability over a range of carbon contents. Figure 10 shows Jominy end-quench data for the core and for all carbon levels up to 0.9% for an SAE 4620 carburizing steel. The powerful, beneficial effect of increasing carbon on hardenability is shown. Nevertheless, in heavy sections, where cooling rates are low, even case regions may transform to microstructures other than martensite. Jatczak (Ref 27) has evaluated the effects of various alloying elements on the hardenability of high-carbon steels and has shown that higher austenitizing temperatures increase hardenability by dissolving alloy carbides and increasing the amount of carbon and alloying elements in solution in the austenite. Other investigators have also evaluated various aspects of the hardenability of carburized steels (Ref 28–31).

Other Alloy Effects. Although hardenability is a major concern in alloying and the selection of carburizing steels, alloy elements also affect other aspects of microstructure. Many of the alloying elements, in particular chromium and molybdenum, are strong carbide and ferrite formers. Those elements shift A_{cm} temperatures (Fig 11) and raise Ae_1 temperatures, the lowest temperatures at which austenite is stable under equilibrium conditions. The shift in A_{cm} by carbide-forming elements limits the amount of carbon that can be dissolved in austenite and increases the possibility of carbide formation in carburized steels.

Many alloying elements also lower M_s temperatures and the transformation temperature ranges for martensite formation (Ref 16, 33). Therefore increased alloying increases the amounts of austenite that are retained in carburized and hardened steels.

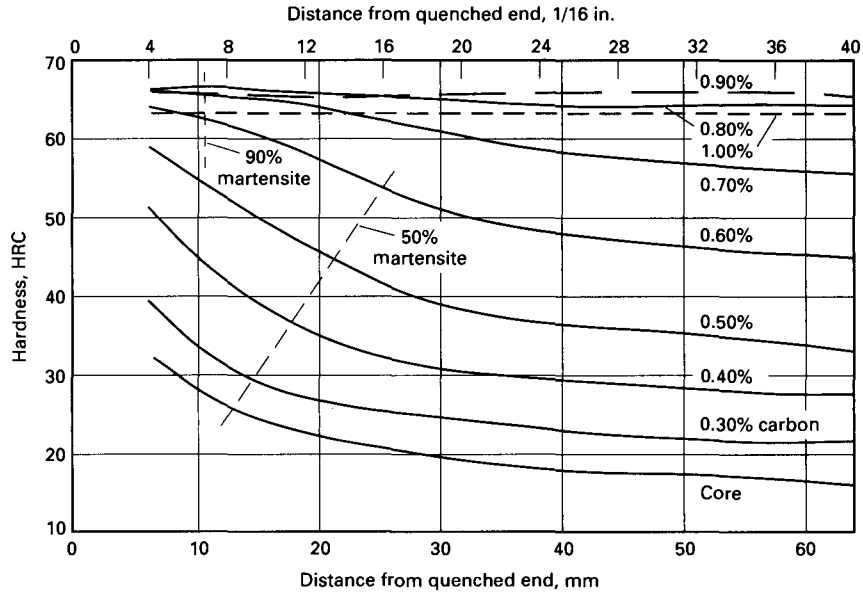

Fig 10 Jominy end-quench curves showing hardenability differences as a function of carbon content in direct-quenched SAE 4620 steel. Source: Ref 2

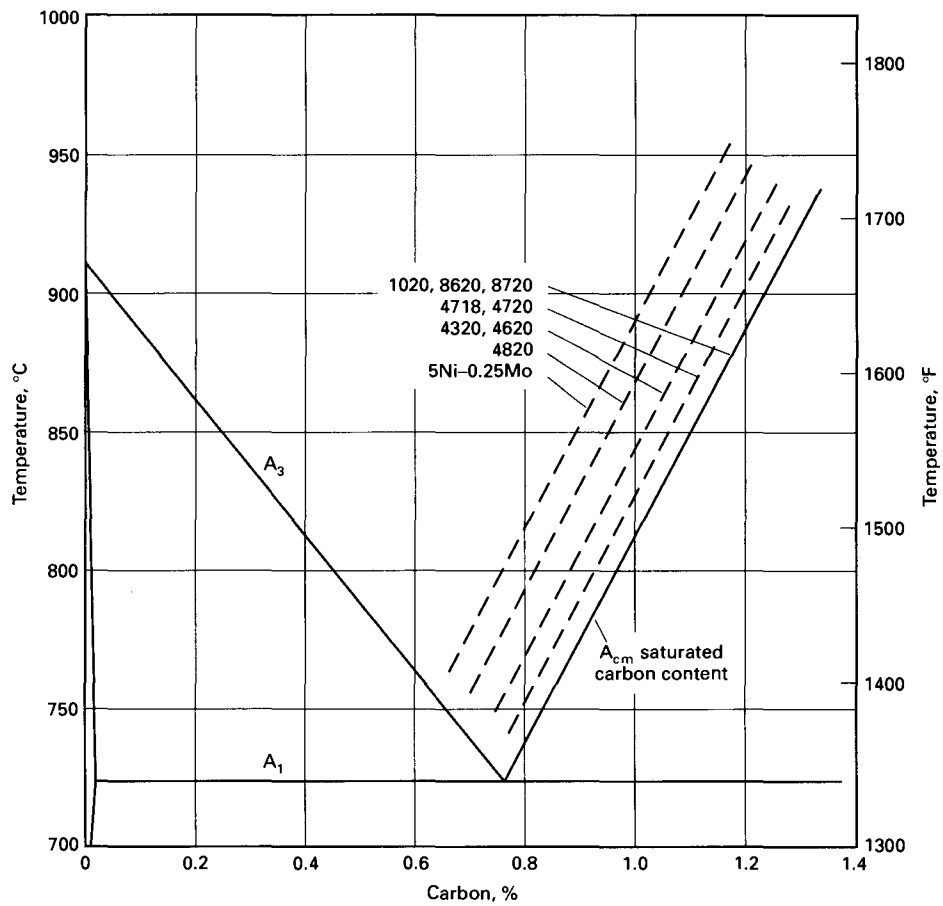

Fig 11 The shift in A_{cm} temperatures with alloying in various carburizing steels. Source: Ref 32

Intergranular Fracture at Austenite Grain Boundaries

Figure 12 shows an example of intergranular fracture at prior austenite grain boundaries in the case overload fracture zone of a carburized 8620 steel. Such intergranular cracking is a major fracture mode of high-carbon hardened steels that have been quenched from temperatures at which the microstructure consists only of polycrystalline austenite. Thus cracking can occur in the case regions of steel directly quenched after carburizing, but rarely in carburized steels that have been reheated to produce finer-grained structures with retained carbides (Ref 17, 22). Fracture in the latter microstructures is low-toughness ductile fracture characterized by closely spaced microvoids that form around the dispersed carbide particles. Intergranular fracture occurs even in carburized steels tempered between 150 and 200 °C (300 and 400 °F),

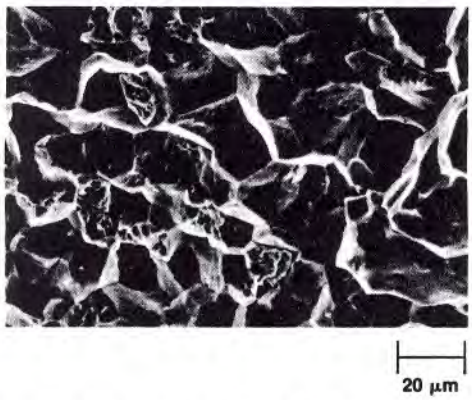

Fig 12 Intergranular fracture from the overload fracture zone in the case of a carburized SAE 8620 steel. Scanning electron microscope (SEM) micrograph. Source: Ref 14

tempering temperatures that are too low to cause tempered martensite embrittlement (Ref 16).

The reasons for the intergranular fracture of high-carbon case microstructures have been difficult to establish because no associated grain-boundary features are discernible in the light microscope. However, several studies suggest that the sensitivity to grain-boundary fracture is due to a two-step process (Ref 17, 34, 35): first, the segregation of phosphorus to austenite grain boundaries during carburizing or austenitizing for hardening and, second, the nucleation and growth of very thin cementite particles on austenite grain boundaries during quenching. The phosphorus segregation and carbide formation are largely on an atomic scale, but their combined effect is sufficient to produce interfaces that fracture at lower stresses than do the matrix martensite and austenite.

The key to the identification of microstructural features leading to intergranular fracture has been the application of Auger electron spectroscopy (AES), an analytical technique that has very high depth resolution. Auger electrons of specific energies are emitted from specific atoms on a surface that is irradiated with an electron beam in a high vacuum chamber. The Auger electrons have very low energy and originate from a depth of less than 1 nm from the surface of a specimen (Ref 36).

Figure 13 shows Auger spectra from case fracture surfaces of a carburized 8620 steel. The spectra in Fig 13(a) is from a transgranular fracture surface, while that in Fig 13(b) is from an intergranular fracture surface. No phosphorus peak is detectable in the spectrum produced from the transgranular fracture, and a small phosphorus peak, clearly shown by the 10× magnification, is produced from the intergranular fracture surface. These observations are consistent with other investigations that show that phosphorus segregates to austenite grain boundaries during austenitizing (Ref 35, 37).

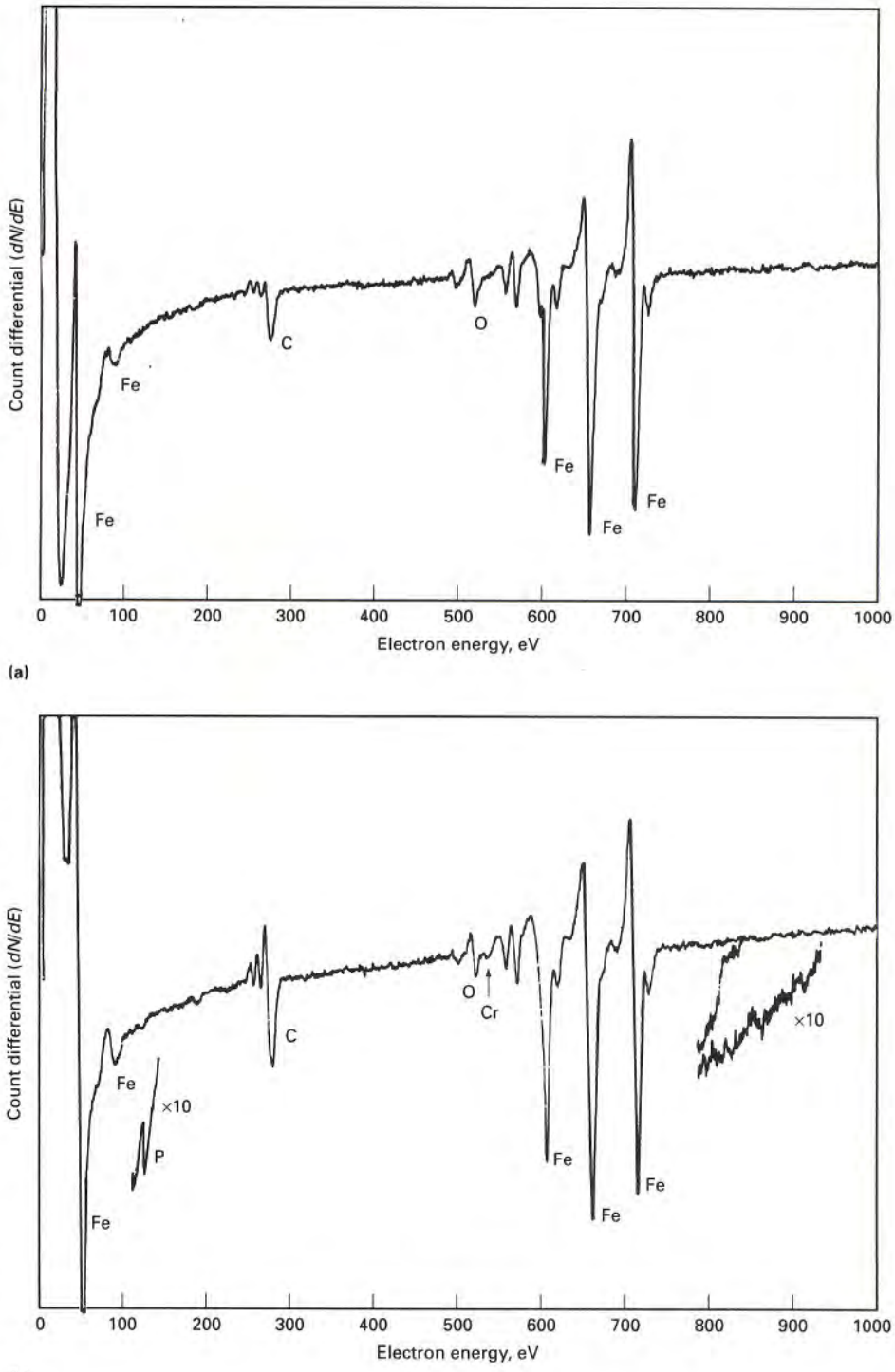

Fig 13 Auger electron spectra from case fracture surfaces of carburized 8620 steel. (a) From transgranular fracture surface. (b) From intergranular fracture surface. Source: Ref 17

A major difference between the two spectra is the significantly larger carbon peak in the Auger spectrum from the intergranular fracture surface. The carbon peak shape, characterized by a major peak and several auxiliary peaks, is identical to that produced by AES of cementite (Ref 35). Thus AES analysis provides evidence for cementite formation on austenite grain boundaries.

A fracture toughness study on a set of EX24-type steels (or SAE 4121) containing 0.85% C with 0.044 and 0.002% P verified the above observations (Ref 34). The high carbon content was designed to simulate the high-carbon case of carburized specimens. High phosphorus content greatly increased the amount of intergranular fracture. Intergranular fracture was significantly reduced, but not

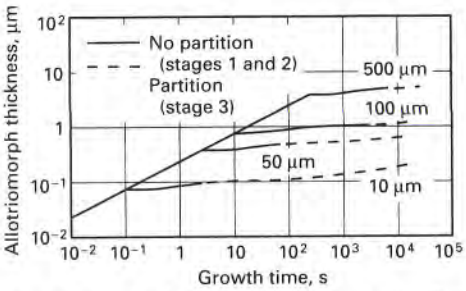

Fig 14 Simulated growth curves for cementite allotriomorph formation on austenite grain boundaries in an iron-chromium-carbon alloy (Fe, 4.5 at.% C, 1.5 at.% Cr) at 740 °C (1365 °F). Source: Ref 38

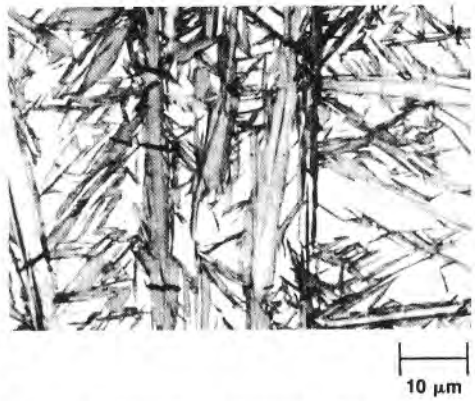

Fig 15 Microcracks in martensite plates of an Fe-1.86C alloy. Light micrograph. Source: Ref 42

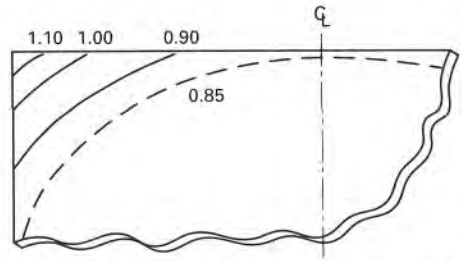

Fig 16 Schematic of carbon concentrations at the corners of an 8620 steel specimen subjected to carburizing and diffusion at 1050 °C (1920 °F). Based on chemical analysis of chips milled from various locations of the specimen. Source: Ref 49

completely eliminated, in the low-phosphorus steel. Oil-quenched specimens developed more intergranular fracture than brine-quenched specimens, a result explained by increased coverage of austenite grain boundaries by cementite due to more time for diffusion during quenching at slower rates.

Ando (Ref 38, 39) has modelled the growth kinetics of cementite allotriomorphs in high-carbon, iron-chromium-carbon alloys. Figure 14 shows that growth takes place in several stages. At first, rapid thickening occurs in a stage controlled only by carbon diffusion, and no partitioning of chromium takes place. However, equilibrium considerations eventually require the diffusion of chromium to the carbide particles, and at that stage the growth of grain-boundary cementite slows significantly. Therefore, the formation of very thin cementite particles, even during the oil quenching of carburized steels, is explained by the very rapid first-stage growth, shown in Fig 14. High phosphorus content has also been shown to accelerate the formation of cementite grain-boundary allotriomorphs (Ref 35).

Prevention of Intergranular Fracture. As described later in the section "Fatigue Mechanisms," intergranular fracture frequently initiates fatigue cracks in carburized steels. Lower phosphorus contents would reduce intergranular cracking, but the reduction of phosphorus to extremely low levels that might completely eliminate intergranular cracking is dependent on the economics of steelmaking. Reheating carburized specimens with nominal phosphorus contents to produce very fine austenite grain sizes eliminates intergranular cracking (Ref 18, 20), perhaps because of the dilution of phosphorus segregation by a high grain-boundary area. Finally, alloying might be used to eliminate intergranular fracture. Carburizing steels with high nickel contents have high toughness and do not seem to be sensitive to intergranular fracture (Ref 40, 41).

Microcracking in Carburized Steels

Microcracks frequently form in martensite plates of high-carbon steels. Examples of martensite microcracks are shown in Fig 15. Marder and Benscoter have shown by serial metallographic sectioning that the cracks form at points of contact between impinging martensite plates (Ref 43). Because the microcracks are formed by the impingement of nonparallel plates of martensite, microcracking density decreases with the transition from plate to lath martensite (Ref 44). Fine austenite grain size also limits microcracking (Ref 42, 45), apparently because smaller martensite plates do not create sufficient stresses to produce cracks.

Microcracks have long been known to be present in the case microstructures of carburized steels (Ref 18, 46, 47), especially in coarse-grained microstructures with large martensite plates. The presence of microcracks may contribute to impaired fatigue performance of carburized steels. However, microcracks may have only a very secondary effect on fatigue, in light of the fact that many fatigue cracks initiate at embrittled austenite grain boundaries, as discussed in the previous section. Such grain-boundary cracks effectively bypass the microcracked martensite plates within austenite grains, and therefore the presence or absence of microcracks is immaterial to fatigue crack initiation. On the other hand, the influence of microcracks in martensite plates on transgranular crack propagation would be expected.

A study of grain size effects on microcracking in an Fe-1.22% C alloy provides a link between microcracking and grain-boundary fracture (Ref 45). In that study microcracks were found both in martensite plates and at prior austenite grain boundaries. As grain size decreased, both types of microcracks decreased, but the number of grain-boundary microcracks became a higher fraction of the total. The intergranular microcracks may have formed partly because of martensite plate impingement on embrittled grain boundaries. If such grain-boundary microcracks are present in carburized steels, intergranular fatigue crack initiation will occur at lower stresses.

Excessive Retained Austenite and Massive Carbides

Moderate amounts of retained austenite are proper and unavoidable in the high-carbon case microstructure of carburized steels. However, excessive amounts of retained austenite, that is, greater than 50%, lower hardness significantly and reduce bending fatigue resistance. The most important cause of excessive amounts of retained austenite is too high a surface carbon content. This condition drives M_s temperatures down and shifts the balance of the temperature range for martensite transformation to well below room temperature. High alloy content also lowers M_s temperatures.

Common locations of excessive surface carbon concentration are specimen corners at which the austenite is saturated with carbon during the first part of a carburizing cycle (Ref 48, 49). The carbon has access to both surfaces of the corner during carburizing but has little physical access to the interior of the specimen during the diffusion part of a cycle. As a result, although carbon content falls to desired levels on the flat or gradually curved surfaces of a part, the carbon content at a corner remains much higher than desired. Figure 16 shows carbon contours determined at the corners of an 8620 steel specimen carburized at 1050 °C (1920 °F). Carbon contents as high as 1.20% were measured at the corner. Excessive retained austenite in the corner microstructure of a 4121 carburized specimen is shown in Fig 17. Figure 18 shows hardness profiles from corner and plane surface regions of 8620 steel carburized at 930 °C (1700 °F). The corner surface hardness is much lower than that of the plane surface because of high retained austenite content. Reheating of direct-quenched specimens eliminates excessive retained austenite and raises surface hardness (Ref 48, 49).

Another consequence of too high a surface carbon content is the formation of massive carbides. The carbides form at austenite grain boundaries and may have different morphologies, depending on alloy content. As discussed relative to Fig 14,

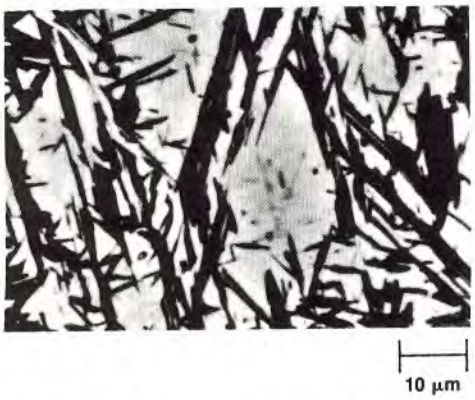

Fig 17 High retained austenite content in corner of SAE 4121 steel (formerly EX24) specimen carburized at 1050 °C (1920 °F). Source: Ref 44

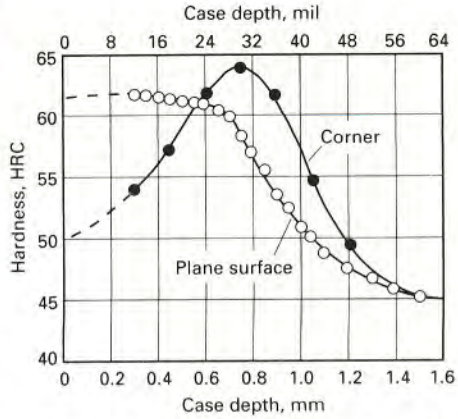

Fig 18 Corner and plane surface microhardness profiles from 8620 steel specimen carburized at 930 °C (1700 °F). Source: Ref 48

large carbide grain-boundary allotriomorphs require considerable diffusion to grow, and therefore they form during the high-temperature stages of carburizing or when the temperature of the part is lowered to about 845 °C (1550 °F) just prior to quenching. Figure 19 shows two morphologies of massive carbides that have formed in the corners of carburized specimens. Figure 19(a) shows blocky, angular particles formed in an 8620 steel containing nominally 0.5% Cr, 0.5% Ni, and 0.2% Mo. Figure 19(b) shows long, thin carbides formed in an SAE 4121 steel containing 0.55% Cr and 0.24% Mo but no nickel.

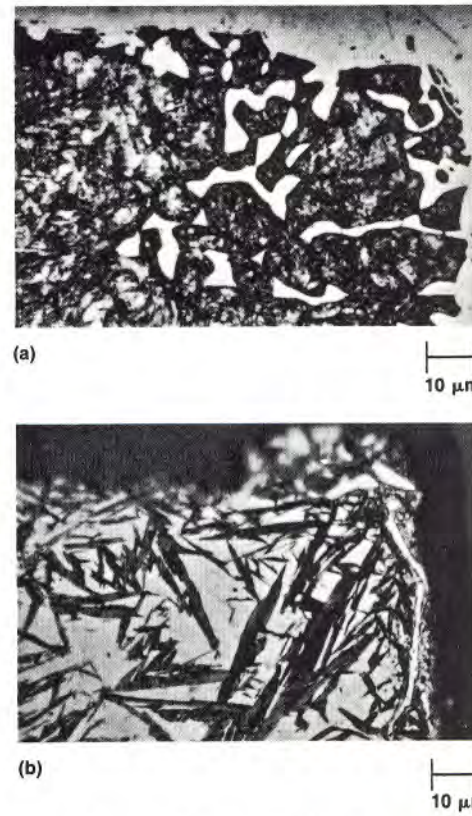

Fig 19 Examples of massive carbides formed at the corners of carburized specimens. (a) Blocky carbides in 8620 steel. (b) Thin, continuous grain-boundary carbides in SAE 4121 steel. Light micrographs. Source: Ref 49

Effect on Fatigue Cracking. The combination of excessive retained austenite and massive carbides, together with stress concentration at sharp changes in section, causes fatigue crack initiation at specimen corners. Figure 20(a) shows fatigue initiation at the corner of a carburized specimen of SAE 4121 steel. Details of the corner fracture along the massive carbides are shown in Fig 20(b). Carbide grain-boundary allotriomorphs grow by ledges, which make up the interface between the carbides and the martensite-austenite matrix (Ref 39). These ledges provide preferred fracture paths, as shown in Fig 20(b).

Although massive network carbides are detrimental to the bending fatigue and fracture performance of carburized steels in many applications, a process referred to as super carburizing is occasionally used for special applications (Ref 50). This process supersaturates a part surface with carbon and results in the formation of large volumes of massive carbide particles. Surface carbon contents of 1.80% to greater than 3.0% are produced, and steels with large amounts of carbide-forming elements such as chromium and molybdenum respond most effectively. High volume fractions of hard alloy carbide particles significantly increase resistance to abrasive wear, but also may create problems in the grinding of the very hard surfaces.

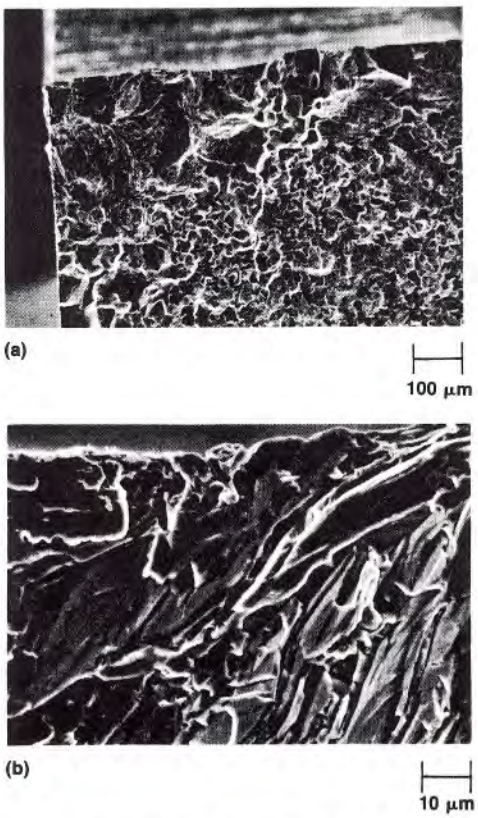

Fig 20 Fracture surfaces of carburized SAE 4121 steel. (a) Low-magnification view of corner initiation. (b) Detail of fracture at carbide-matrix interface. SEM micrographs. Source: Ref 48

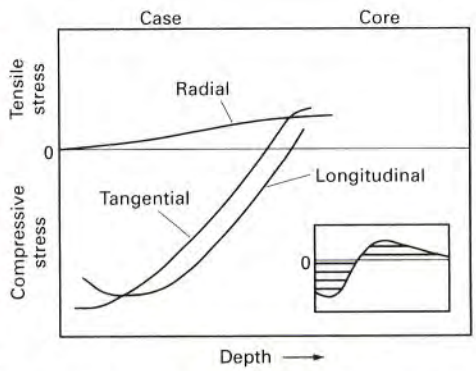

Fig 21 Schematic diagram of residual stresses in carburized steels. Insert shows that surface compressive residual stresses are balanced by interior tensile stresses. Source: Ref 8

Residual Stresses

A major benefit of carburizing is the introduction of compressive residual stresses into the surfaces of carburized parts. These stresses counteract applied tensile stresses and therefore improve bending fatigue performance. Because of the importance of residual stresses to the performance of carburized parts, considerable effort has been devoted to modelling, measuring, and understanding their effects (Ref 1, 7, 8, 51-54).

Figure 21 shows schematically the residual stress profiles that develop in properly carburized and hardened steels. The compressive stresses reach a maximum at some distance from the surface, gradually decrease, and are eventually balanced by tensile residual stresses in the core of the carburized part. A survey of a number of carburized parts showed that measured

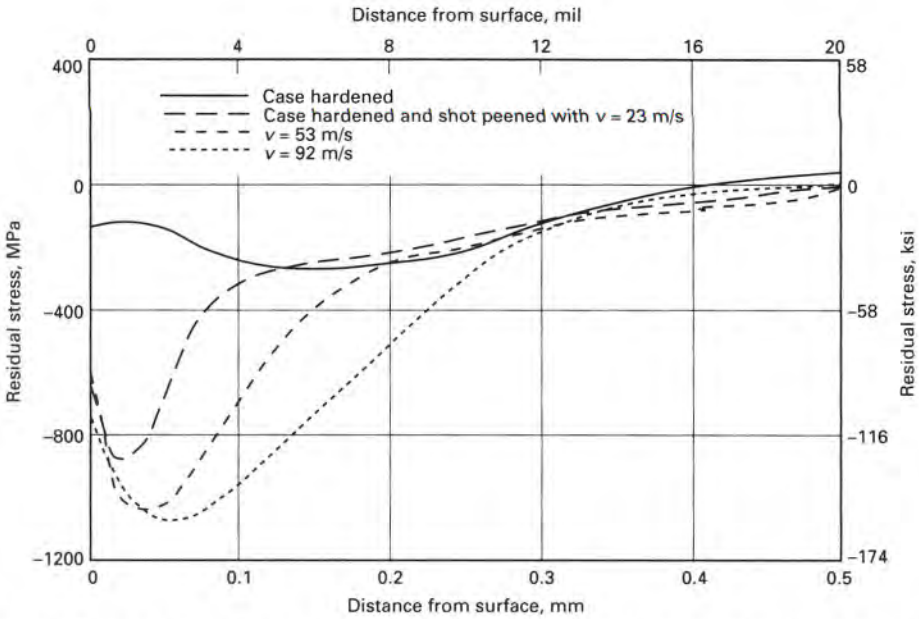

Fig 22 Effect of shot peening at different velocities on compressive residual stresses in carburized 16MnCr5 steel (1.23% Mn, 1.08% Cr). Source: Ref 52

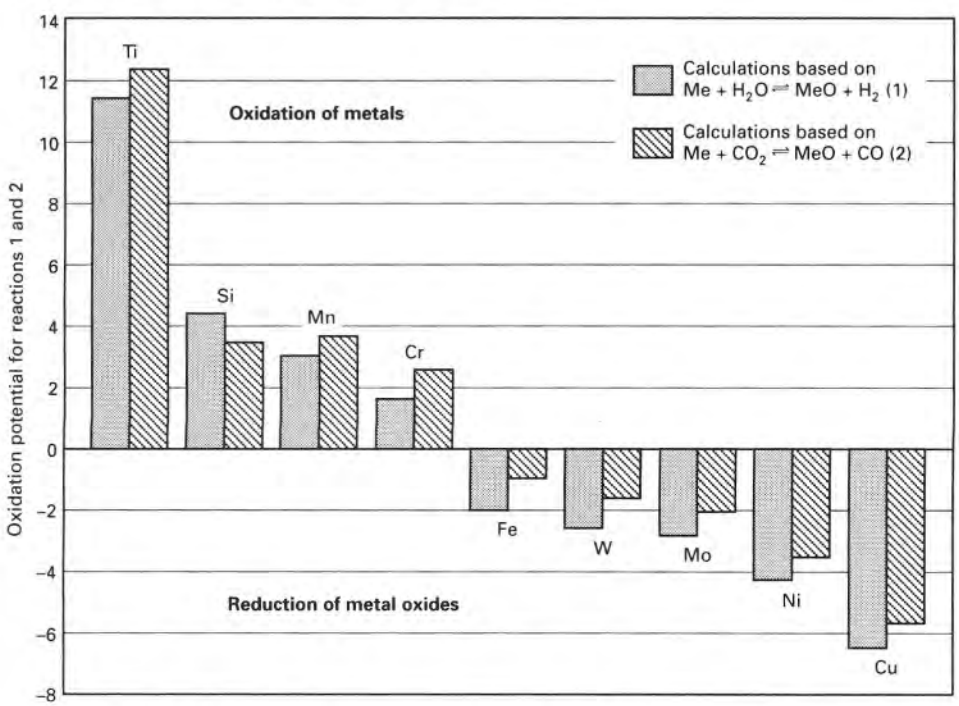

Fig 23 Oxidation potentials of various alloying elements and iron in an endothermic gas atmosphere at 930 °C (1700 °F). Source: Ref 60

peak compressive stresses ranged from −200 to −450 MPa (−29 to −65 ksi) (Ref 8).

Surface compressive residual stresses in carburized steels arise from transformation and temperature gradients induced during cooling and the volume expansion that accompanies the transformation of austenite to martensite (Ref 55). The carbon profiles produced by carburizing introduce the M_s temperature and transformation gradients: the M_s temperature is lowest at the surface, where carbon content is the highest, and increases with increasing distance from the surface as carbon content approaches that of the core. Temperature gradients are due to heat flow and thermal-conductivity factors; at any given time during quenching, the surface temperature is lower than temperatures in the part interior.

In the early stages of cooling, martensite first forms at some distance from the surface, where the part temperature has fallen

Fig 24 Internal oxidation (dark features) at surface of gas-carburized steel containing 1.06% Mn, 0.21% Si, 0.52% Cr, 0.50% Ni, and 0.17% Mo. Light micrograph. Source: Ref 20

below the higher, interior M_s temperatures. The volume changes at this stage are readily accommodated by the surrounding austenite because of its low flow stresses and the high temperatures. The surface austenite does not transform because of its low M_s. The temperature continues to fall and eventually drops below the M_s in the surface regions. The expansion at this point is constrained by the interior martensite that has formed earlier, and as a result the surface microstructure is placed in compression. Many factors affect this process, including alloy and carbon levels, which set hardenability and M_s temperatures; case depths; temperature at the start of quenching; quenchant temperature; and the temperature-dependent plastic flow behavior of martensite and austenite. Despite the complexity of the interactions that affect the formation of residual stresses, hardened carburized parts with the martensite-austenite microstructures described earlier generally develop favorable compressive stresses.

Surface compressive residual stresses can be increased by shot peening. Figure 22 shows the dramatic effect of shot peening at different velocities on the compressive residual stresses of carburized steel. These improvements in stresses translate into improved bending fatigue performance.

Residual stresses can be adversely affected by surface oxidation during gas carburizing. As discussed in the next section, certain alloying elements are preferentially oxidized and removed from solid solution in the austenite. As a result, hardenability decreases, and, in severe cases, pearlite instead of martensite forms at the surface (Ref 56). Thus the surface transformation occurs at high temperatures, and the beneficial effect of austenite-to-martensite transformation late in the quenching process is lost. Even if the oxidation is not severe enough to cause pearlite formation, surface M_s temperatures may be raised by the removal of some of the alloying

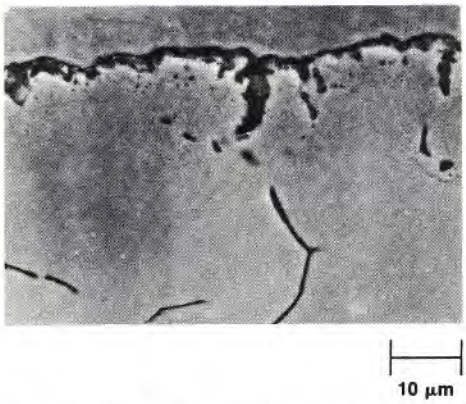

Fig 25 Internal oxidation of gas-carburized 20MnCr5 steel containing 1.29% Mn, 0.44% Si, 1.25% Cr, 0.25% Ni, and 0.0015% B. SEM micrograph. Source: Ref 61

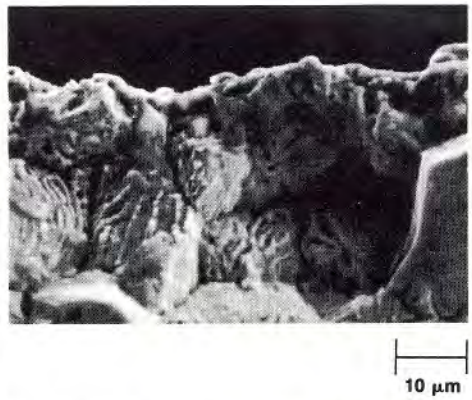

Fig 26 Lamellar internal grain-boundary oxides on fracture surface of carburized 20MnCr5 steel containing boron. SEM micrograph. Source: Ref 61

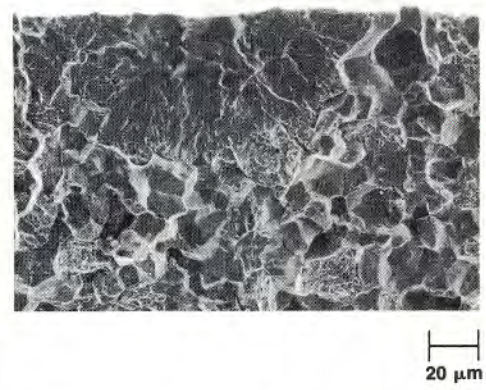

Fig 27 Example of type 1 bending fatigue fracture initiation consisting of short intergranular crack initiation site, a region of transgranular crack propagation, and overload intergranular fracture through case. Plasma-carburized steel containing 1.06% Mn, 0.52% Cr, 0.30% Ni, and 0.1% Mo. SEM micrograph. Source: Ref 20

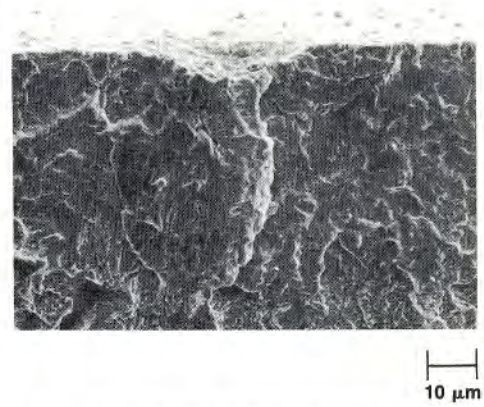

Fig 28 Example of type 2 bending fatigue fracture initiation consisting of transgranular initiation and propagation, with gas-carburized 8719 steel. SEM micrograph. Source: Ref 20

element, resulting in a thin surface zone with lower compressive stresses.

Subzero, or cryogenic refrigeration is sometimes used to lower retained austenite contents (Ref 7). As a result, surface hardness increases. Also, dimensional stability in service is increased because there is less austenite available to transform to martensite by stress- or strain-controlled mechanisms. However, a number of investigations have shown that the refrigeration treatment of carburized parts lowers fatigue performance (Ref 48, 57, 58). The transformation of additional surface retained austenite would be expected to continue the process established during quenching to room temperature; that is, the volume expansion associated with the formation of new martensite would be constrained, and compressive stresses would be increased. Increased compressive stresses are in fact measured in the martensite of refrigerated specimens (Ref 7, 57, 58). However, Kim *et al.* (Ref 57) have shown that the stresses in the remaining retained austenite are tensile. Such localized tensile stresses would lower the applied stresses required to initiate and propagate fatigue cracks.

Surface and Internal Oxidation

The H_2O/H_2 and CO_2/CO equilibria in gas carburizing atmospheres cause the internal oxidation of certain alloying elements in carburizing steels (Ref 7, 59). Figure 23 shows the oxidizing potentials for various elements in endothermic gas at 930 °C (1700 °F). Chromium, silicon, and manganese, all commonly found in carburizing steels, oxidize readily, while molybdenum, nickel, and iron are not oxidized. The oxidation is diffusion dependent, and therefore the depth and extent of oxide formation is a function of carburizing time and temperature. The oxides may form on austenite grain boundaries or within austenite grains.

Figure 24 shows internal oxidation at the surface of a carburized specimen of a steel containing 1.06% Mn, 0.21% Si, 0.52% Cr, 0.50% Ni, and 0.17% Mo. The oxidation has followed the austenite grain boundaries to a depth on the order of an austenite grain diameter, about 10 μm (0.4 mil). This depth of penetration is typical for steels carburized to a case depth of about 1 mm (40 mil).

Figure 25 shows the surface oxidation of a carburized 20MnCr5 steel containing 1.29% Mn, 0.44% Si, 1.25% Cr, 0.25% Ni, and 0.0015% B. There are two zones of oxidation. The outer zone, about 5 μm (0.2 mil) deep, consists of chromium-rich oxides penetrating into the austenite grains. The other zone, about 30 μm (1.2 mils) deep, consists of manganese-rich and silicon-rich oxides along austenite grain boundaries. These oxide chemistries and morphologies agree with those presented by Chatterjee-Fischer (Ref 59). In addition, silicon appears to form intergranular dispersed oxide particles.

The grain-boundary oxides shown in Fig 25 appear to be discontinuous. Examination of fractured specimens of the same carburized steel shown in Fig 25 showed that the intergranular oxides grew as lamellae (Fig 26). Thus the oxide structure appears to develop by a discontinuous or cellular transformation in which grain-boundary austenite initially containing nominal amounts of silicon and manganese decomposes to alloy oxides and austenite depleted in silicon and manganese. The discontinuous appearance of the oxides in Fig 25 is therefore due to a sectioning effect through the oxide and austenite lamellae.

The effect of internal oxidation on fatigue performance depends on the degree of oxidation. As noted in the section on residual stresses, if sufficient depletion of the alloying elements occurs, hardenability may decrease to the point at which pearlite and other nonmartensitic transformation products form. The latter surfaces have low hardness, tensile residual surface stresses, and reduced fatigue performance (Ref 56, 62, 63). The reduced surface hardness of some oxidized carburized steels has also been attributed to the decarburization that accompanies internal oxidation (Ref 64).

If the depth and degree of internal oxidation is limited, and if the surface structure of a carburized steel consists of martensite-austenite mixtures with surface residual compressive stresses, then there is little or no effect of intergranular oxidation on fatigue performance. Parrish (Ref 7) discussed evidence showing that oxidation less than 13 μm (0.5 mil) deep has little effect on fatigue. Pacheco and Krauss (Ref 20) showed that very good fatigue resistance could be attained in carburized specimens with the internal oxidation shown in Fig 24, provided that the surface martensite-austenite microstructure formed in fine-grained austenite.

Fatigue Mechanisms

Identification of the best compositions and best microstructures for the production of carburized steels with high fatigue resistance has been difficult. All of the microstructural features described in the preceding sections influence fatigue performance.

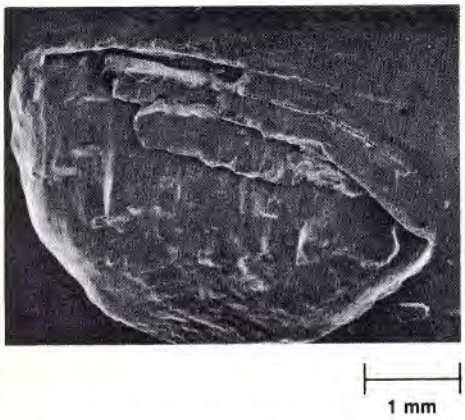

Fig 29 An example of spalling in carburized SAE 4118 steel subjected to rolling contact loading. Courtesy of R. Miller, Colorado School of Mines, and T. Clements, Caterpillar Inc.

Many of the earlier studies that ranked various alloy steels reported relatively modest bending fatigue strengths, between 700 and 1000 MPa (100 and 145 ksi) (Ref 65, 66). Claims for the benefits of various alloying elements have been made, but little detailed microstructural and fractographic analysis has been performed to correlate mechanisms with benefits of alloying. Nevertheless, the results of studies that show low-to-moderate fatigue strengths probably reflect the properties of commercial carburized parts that are overwhelmingly successful in service because of conservative mechanical design. However, failures do occur (Ref 13, 67), and the causes, sometimes obvious, sometimes subtle, must be identified in order to improve consistently the future performance of carburized parts.

A few studies have shown that very high bending fatigue limits (≥1400 MPa, or 200 ksi) can be achieved in carburized steels under conditions of tension-tension cyclic (R = 0.1) loading (Ref 18, 20, 68, 69). Moreover these studies are beginning to identify microstructures associated with various ranges of fatigue performance. Polished surfaces to eliminate machining marks and other surface flaws, as well as rounded specimen corners or specimen designs that minimize edge effects, are necessary to eliminate fatigue initiation sites which obscure the effects of microstructure.

From the standpoint of microstructures, based on experimental fatigue studies (R = 0.1), there appear to be two major mechanisms of bending fatigue crack initiation. For conciseness, these two mechanisms are defined and referred to as type 1 and type 2 in the following discussion. Type 1 is associated with intergranular fatigue initiation at austenite grain boundaries with phosphorus-carbide structures. This mechanism is typically observed in direct-quenched carburized specimens and is associated with endurance limits up to 1260 MPa (183 ksi) (Ref 12). Thus quite reasonable levels of fatigue performance can be attained in carburized steels with a sensitivity to grain-boundary fracture. The other mechanism, type 2, is associated with transgranular fatigue crack initiation and correlates with bending fatigue endurance limits greater than 1400 MPa (200 ksi). Figure 27 shows an example of type 1 initiation, and Fig 28 shows an example of type 2 initiation.

Zaccone *et al.* (Ref 70, 71), working with simulated case microstructures, have shown that in type 1 initiation, small grain-boundary cracks form very early in the fatigue cycle, perhaps in the first cycle if the applied stresses are high enough to reach the threshold of grain-boundary cracking. This crack is arrested after traveling the length of only a few grains. The strain-induced transformation of retained austenite to martensite at the crack tip occurs and apparently creates compressive residual stresses that halt the crack (Ref 70-72). For this reason, retained austenite is beneficial for prolonging fatigue life under conditions of low-cycle, high strain fatigue. Although fatigue crack propagation rates are slowed by high retained austenite contents, fracture eventually occurs when a sufficient number of accumulated cycles cause the crack to reach the critical size for unstable overload fracture. Once the intergranular crack is arrested, propagation proceeds by transgranular cracking (Fig 27). Overload fracture of specimens sensitive to type 1 initiation also tends to be largely intergranular until lower-carbon martensite is encountered.

Type 2, transgranular fatigue crack initiation, is dependent on slip mechanisms of crack formation during cyclic loading (Ref 73). Thus, a key feature of this mechanism, in contrast to type 1 initiation, is that a crack is not immediately generated during the first loading cycles. Cycle-dependent transgranular crack initiation develops in fine-grained case microstructures where conditions for intergranular cracking are mitigated. Low amounts of retained austenite or finely distributed retained austenite also favor type 2 initiation and therefore contribute to high performance under conditions of high-cycle fatigue because slip is more difficult in fine, largely martensitic microstructures (Ref 20, 70, 71).

Contact Fatigue Resistance of Gears and Bearings. Carburized steels in applications such as bearings and gears must also be resistant to rolling-contact fatigue (Ref 8, 13, 19, 67). The stresses that initiate failure under contact conditions are shear stresses that peak at some distance below the surface. Therefore cracks that lead to spalling develop at subsurface microstructural discontinuities such as oxide inclusion particles. Extreme cases of spalling are associated with case crushing or cracking initiated at the case-core interface. Figure 29 shows an example of a spall on a carburized SAE 4118 interface. If sliding is coupled with contact loading, surface pits develop. Very high contact loads cause microstructural changes within high-carbon martensite that are revealed by various types of etching (Ref 74-76). Generally retained austenite is regarded as a microstructural constituent that is beneficial for rolling-contact fatigue resistance (Ref 77, 78).

REFERENCES

1. D.E. Diesburg, Ed., *Case-Hardened Steels: Microstructural and Residual Stress Effects*, TMS-AIME, 1984
2. D.V. Doane, Carburized Steel—Update on a Mature Composite, in *Carburizing: Processing and Performance*, G. Krauss, Ed., ASM International, 1989, p 169-190
3. *Carburizing and Carbonitriding*, ASM Committee on Gas Carburizing, American Society for Metals, 1977
4. H.E. Boyer, Ed., *Case Hardening of Steel*, ASM International, 1987
5. J. Grosch and J. Wunning, Ed., *Einsatzharten*, Arbeitsgemeinschaft Warmebehandlung und Werkstofftechnik, 1989. Some articles from this Proceedings have been reprinted in *Härt.-Tech. Mitt.*, Vol 45 (No. 2), 1990
6. G. Krauss, Ed., *Carburizing: Processing and Performance*, ASM International, 1989
7. G. Parrish, *The Influence of Microstructure on the Properties of Case-Carburized Components*, American Society for Metals, 1980
8. G. Parrish and G.S. Harper, *Production Gas Carburizing*, Pergamon Press, 1985
9. C.A. Stickels and C.M. Mack, Overview of Carburizing Processes and Modeling, in *Carburizing: Processing and Performance*, G. Krauss, Ed., ASM International, 1989, p 1-9
10. U. Wyss, Grundlagen des Einsatzhartens, *Härt.-Tech. Mitt.*, Vol 45, 1990, p 44-56
11. J.I. Goldstein and A.E. Moren, Diffusion Modeling of the Carburization Process, *Metall. Trans. A*, Vol 9A, 1978, p 1515-1525
12. K.A. Erven, "The Effects of Sulfur and Titanium on Bending Fatigue Performance of Carburized Steels," M.S. thesis, Colorado School of Mines, 1990
13. L.E. Alban, *Systematic Analysis of Gear Failures*, American Society for Metals, 1985
14. K.D. Jones, "Effects of Partial Pressure Carburizing on the Microstructure and Bending Fatigue Behavior of SAE 8620 and EX24 Steels," M.S. thesis, Colorado School of Mines, 1978
15. G. Krauss and A.R. Marder, The Morphology of Martensite in Iron Alloys, *Metall. Trans.*, Vol 2, 1971, p 2343-2357

16. G. Krauss, *Steels, Heat Treatment and Processing Principles*, ASM International, 1990
17. G. Krauss, The Microstructure and Fracture of a Carburized Steel, *Metall. Trans. A*, Vol 9A, 1978, p 1527-1535
18. C.A. Apple and G. Krauss, Microcracking and Fatigue in a Carburized Steel, *Metall. Trans.*, Vol 4, 1973, p 1195-1200
19. V.K. Sharma, G.H. Walter, and D.H. Breen, An Analytical Approach for Establishing Case Depth Requirements in Carburized Gears, *J. Heat Treat.*, Vol 1 (No. 1), 1979, p 20-29
20. J.L. Pacheco and G. Krauss, Microstructure and High Bending Fatigue Strength in Carburized Steel, *J. Heat Treat.*, Vol 7, 1989, p 77-86; also, in *Härt.-Tech. Mitt.*, Vol 45, 1990, p 77-84
21. D.L. Yaney, "The Effects of Phosphorus and Tempering on the Fracture of AISI 52100 Steel," M.S. thesis, Colorado School of Mines, 1981
22. G. Krauss, The Relationship of Microstructure to Fracture Morphology and Toughness of Hardened Hypereutectoid Steels, in *Case Hardened Steels: Microstructure and Residual Stress Effects*, TMS-AIME, 1984, p 33-56
23. D.V. Doane and J.S. Kirkaldy, Ed., *Hardenability Concepts with Applications to Steel*, American Institute of Mining, Metallurgical, and Petroleum Engineers, 1978
24. C.A. Siebert, D.V. Doane, and D.H. Breen, *The Hardenability of Steels—Concepts, Metallurgical Influences, and Industrial Applications*, American Society for Metals, 1977
25. H. Treppschuh and R. Randak, Verfahren zur Herstellung Besonders Zaher, Borhaltiger Stahle, West German Patent 1608632, 1969
26. W.T. Cook, The Effect of Aluminum Treating on the Case-Hardening Response of Plain Carbon Steels, *Heat Treat. Met.*, Vol 11 (No. 1), 1984, p 21-23
27. C.F. Jatczak, Hardenability of High Carbon Steels, *Metall. Trans.*, Vol 4, 1973, p 2267-2277
28. D.V. Doane and A.T. DeRetana, Predicting Hardenability of Carburizing Steels, *Met. Prog.*, Vol 100 (No. 3), 1971, p 65-69
29. J.M. Tartaglia and G.T. Eldis, Core Hardenability Calculations for Carburizing Steels, *Metall. Trans. A*, Vol 15A, 1984, p 1173-1183
30. D.H. Breen, G.H. Walter, C.J. Keith, and J.T. Sponzilli, Computer Based System Selects Optimum Cost Steels, article series, *Met. Prog.*, Dec 1972, and Feb, April, June, Dec 1973
31. U. Wyss, Kohlenstoff und Harteverlauf in der Einsatzhartungsschicht Verschieden Legierter Einsatzstahle, *Härt.-Tech. Mitt.*, Vol 43, 1988, p 27-35; J.A. Halgren and E.A. Solecki, "Case Hardenability of SAE 4028, 8620, 4620, and 4815 Steels," Technical Paper 149A, Society of Automotive Engineers, 1960
32. Modern Carburized Nickel Alloy Steels, Reference Book Series 11,005, Nickel Development Institute, 1989
33. K.W. Andrews, Empirical Formulae for the Calculation of Some Transformation Temperatures, *J. Iron Steel. Inst.*, Vol 203, 1965, p 721-727
34. H.K. Obermeyer and G. Krauss, Toughness and Intergranular Fracture of a Simulated Carburized Case in EX-24 Type Steel, *J. Heat Treat.*, Vol 1 (No. 3), 1980, p 31-39
35. T. Ando and G. Krauss, The Effect of Phosphorus Content on Grain Boundary Cementite Formation in AISI 52100 Steel, *Metall. Trans. A*, Vol 12A, 1981, p 1283-1290
36. J.I. Goldstein and H. Yakowitz, *Practical Scanning Electron Microscopy*, Plenum Press, 1975, p 87-91
37. H. Ohtani and C.J. McMahon, Jr., Modes of Fracture in Temper Embrittled Steels, *Acta Metall.*, Vol 23, 1975, p 337-386
38. T. Ando, "Isothermal Growth of Grain Boundary Allotriomorphs of Cementite in Ternary Fe-C-Cr Austenite," Ph.D. thesis, Colorado School of Mines, 1982
39. T. Ando and G. Krauss, The Isothermal Thickening of Cementite Allotriomorphs in a 1.5Cr-1C Steel, *Acta Metall.*, Vol 29, 1981, p 351-363
40. D. Wicke and J. Grosch, Das Festigkeitsverhalten von Legierten Einsatzstahlen bei Sclagbeanspruchung, *Härt.-Tech. Mitt.*, Vol 32, 1977, p 223-233
41. B. Thoden and J. Grosch, Crack Resistance of Carburized Steel under Bend Stress, in *Carburizing: Processing and Performance*, G. Krauss, Ed., ASM International, 1989, p 303-310
42. A.R. Marder, A.O. Benscoter, and G. Krauss, "Microcracking Sensitivity in Fe-C Plate Martensite," *Metall. Trans.*, Vol 1, 1970, p 1545-1549
43. A.R. Marder and A.O. Benscoter, Microcracking in Fe-C Acicular Martensite, *Trans. ASM*, Vol 61, 1968, p 293-299
44. M.G. Mendiratta, J. Sasser, and G. Krauss, Effect of Dissolved Carbon on Microcracking in Martensite of an Fe-1.39 pct C Alloy, *Metall. Trans.*, Vol 3, 1972, p 351-353
45. R.P. Brobst and G. Krauss, The Effect of Austenite Grain Size on Microcracking in Martensite of an Fe-1.22C Alloy, *Metall. Trans.*, Vol 5, 1975, p 457-462
46. A.H. Rauch and W.R. Thurtle, Microcracks in Case Hardened Steel, *Met. Prog.*, Vol 69, 1956, p 73-76
47. L. Jena and P. Heich, Microcracks in Carburized and Hardened Steel, *Metall. Trans.*, Vol 3, 1972, p 588-590
48. K.D. Jones and G. Krauss, Microstructure and Fatigue of Partial Pressure Carburized SAE 8620 and EX24 Steels, *J. Heat Treat.*, Vol 1 (No. 1), 1979, p 64-71
49. K.D. Jones and G. Krauss, Effects of High-Carbon Specimen Corners on Microstructure and Fatigue of Partial Pressure Carburized Steels, in *Heat Treatment '79*, The Metals Society, 1980, p 188-193
50. R.F. Kern, Super Carburizing, *Heat Treat.*, Oct 1986, p 36-38
51. T. Ericsson, S. Sjostrom, M. Knuuttila, and B. Hildenwall, Predicting Residual Stresses in Cases, in *Case-Hardened Steels: Microstructural and Residual Stress Effects*, D.E. Diesburg, Ed., TMS-AIME, 1984, p 113-139
52. B. Scholtes and E. Macherauch, Residual Stress Determination, in *Case-Hardened Steels: Microstructural and Residual Stress Effects*, D.E. Diesburg, Ed., TMS-AIME, 1984, p 141-151
53. J.A. Burnett, Prediction of Residual Stresses Generated during Heat Treating of Case Carburized Parts, in *Residual Stresses for Designers and Metallurgists*, American Society for Metals, 1981, p 51-69
54. L.J. Ebert, The Role of Residual Stresses in the Mechanical Performance of Case Carburized Steel, *Metall. Trans. A*, Vol 9A, 1978, p 1537-1551
55. D.P. Koistinen, The Distribution of Residual Stresses in Carburized Steels and Their Origin, *Trans. ASM*, Vol 50, 1938, p 227-241
56. B. Hildenwall and T. Ericsson, Residual Stresses in the Soft Pearlite Layer of Carburized Steel, *J. Heat Treat.*, Vol 1 (No. 3), 1980, p 3-13
57. C. Kim, D.E. Diesburg, and R.M. Buck, Influence of Sub-Zero and Shot-Peening Treatment on Impact and Fatigue Fracture Properties of Case-Hardened Steels, *J. Heat Treat.*, Vol 2 (No. 1), 1981, p 43-53
58. M.A. Panhans and R.A. Fournelle, High Cycle Fatigue Resistance of AISI E9310 Carburized Steel with Two Different Levels of Surface Retained Austenite and Surface Residual Stress, *J. Heat Treat.*, Vol 2 (No. 1), 1981, p 55-61
59. R. Chatterjee-Fischer, Internal Oxidation during Carburizing and Heat Treating, *Metall. Trans. A*, Vol 9A, 1978, p 1553-1560
60. I.S. Kozlovskii, A.T. Kalinin, A.J. Novikova, E.A. Lebedeva, and A.I. Festanova, Internal Oxidation during Case-Hardening of Steels in Endothermic Atmospheres, *Met. Sci. Heat Treat.*, No. 3, 1967, p 157-161

61. C. Van Thyne and G. Krauss, A Comparison of Single Tooth Bending Fatigue in Boron and Alloy Carburizing Steels, in *Carburizing: Processing and Performance*, G. Krauss, Ed., ASM International, 1989, p 333-340
62. S. Gunnarson, Structure Anomalies in the Surface Zone of Gas-Carburized Case-Hardened Steel, *Met. Treat. Drop. Forg.*, Vol 30, 1963, p 219-229
63. T. Naito, H. Ueda, and M. Kikuchi, Fatigue Behavior of Carburized Steel with Internal Oxides and Nonmartensitic Microstructures near the Surface, *Metall. Trans. A*, Vol 15A, 1984, p 1431-1436
64. R.L. Colombo, F. Fusani, and M. Lamberto, On the Soft Layer in Carburized Steels, *J. Heat Treat.*, Vol 3 (No. 2), 1983, p 126-128
65. R.A. DePaul, High Cycle and Impact Fatigue Behavior of Some Carburized Gear Steels, *Met. Eng. Q.*, Vol 10, 1970, p 25-29
66. T.B. Cameron, D.E. Diesburg, and C. Kim, Fatigue and Overload Fracture of Carburized Steels, *J. Met.*, 1983, p 37-41
67. D.J. Wulpi, *Understanding How Components Fail*, American Society for Metals, 1985
68. L. Magnusson and T. Ericsson, Initiation and Propagation of Fatigue Cracks in Carburized Steel, in *Heat Treatment '79*, The Metals Society, 1980, p 202-206
69. H. Brandis and W. Schmidt, Contribution to the Influence of Retained Austenite on the Mechanical Properties of Case Hardened Steels, in *Case-Hardened Steels: Microstructural and Residual Stress Effects*, D.E. Diesburg, Ed., TMS-AIME, 1984, p 189-209
70. M.A. Zaccone and G. Krauss, Fatigue and Strain Hardening of Simulated Case Microstructures in Carburized Steels, in *Heat Treatment and Surface Engineering*, G. Krauss, Ed., ASM International, 1988, p 285-290
71. M.A. Zaccone, J.B. Kelley, and G. Krauss, Strain Hardening and Fatigue of Simulated Case Microstructures in Carburized Steel, in *Carburizing: Processing and Performance*, G. Krauss, Ed., ASM International, 1989, p 249-265
72. M.M. Shea, "Impact Properties of Selected Gear Steels," SAE Report 780772, Society of Automotive Engineers, 1978
73. M. Meshii, Ed., *Fatigue and Microstructure*, American Society for Metals, 1979
74. H. Swahn, P.C. Becker, and O. Vingsbo, Martensite Decay during Rolling Contact Fatigue in Ball Bearings, *Metall. Trans. A*, Vol 7A, 1976, p 1099-1110
75. J.A. Martin, S.F. Borgese, and A.D. Eberhardt, Microstructural Alterations of Roller-Bearing Steel Undergoing Cyclic Stresses, *J. Basic Eng.*, 1966, p 555-567
76. V. Bhargava, G.T. Hahn, and C.A. Rubin, Rolling Contact Deformation, Etching Effects, and Failure of High Strength Bearing Steel, *Metall. Trans. A*, Vol 21A, 1990, p 1921-1931
77. C.A. Stickels, Rolling Contact Fatigue Tests of 52100 Bearing Steel Using a Modified NASA Ball Test Rig, *Wear*, Vol 98, 1984, p 199-210
78. L. Kiessling, Rolling-Contact Fatigue of Carburized and Carbonitrided Steels, *Heat Treat. Met.*, Vol 7 (No. 4), 1980, p 97-101